Hindawi
Advances in Civil Engineering
Volume 2020, Article ID 6439207, 10 pages
https://doi.org/10.1155/2020/6439207

Research Article

Nonlinear Dynamic Constitutive Model of Frozen Sandstone Based on Weibull Distribution

Lei Wang, Hongming Su, Shiguan Chen, and Yue Qin

College of Architecture and Civil Engineering, Xi'an University of Science and Technology, Xian, Shaanxi Province, China

Correspondence should be addressed to Hongming Su; 993765278@qq.com

Received 7 February 2020; Revised 3 June 2020; Accepted 6 June 2020; Published 29 June 2020

Academic Editor: Fan Gu

To obtain the dynamic mechanical properties of frozen sandstone at different temperatures (i.e., 20°C, −10°C, −20°C, and −30°C), dynamic uniaxial compression tests of saturated sandstone are conducted using a split-Hopkinson pressure bar. The experimental results demonstrated that the brittleness of the saturated sandstone increased and its plasticity weakened with a decrease in temperature. The peak strength and dynamic elastic modulus of the sandstone were positively correlated with its strain rate. The peak stress was most sensitive to the strain rate at −10°C, and the elastic modulus was most sensitive to the strain rate at −30°C. According to the evident segmentation characteristics of the obtained stress-strain curve, a viscoelastic dynamic constitutive model considering the strain rate effect and temperature effect is developed; this model combines a nonlinear (or linear) body and a Maxwell body in parallel with a damage body. The applicability of the constitutive model is also verified using experimental data. The fitting results were demonstrated to be in good agreement with the experimental results. Furthermore, the fitting results serve as reference for the study of the constitutive model of weakly cemented soft rock and the construction of roadway freezing methods.

1. Introduction

The Jurassic coal seam in western China is covered in thick cretaceous water-rich sandstone. Owing to a special diagenetic process, the sandstone has the mechanical properties of weak cementation, low strength, and large porosity [1–3]. A freezing method is used to stop water and improve the strength of the weak surrounding rocks. However, the freezing wall is often disturbed by drilling and blasting during its construction process, which can result in water seepage and water gushing accidents [4–6]. The main reason for this phenomenon is the damage to the frozen wall caused by blasting impact loads. For example, the failure of the frozen wall of the auxiliary shaft of the no. 1 coal mine in the Shanghai temple, Inner Mongolia, resulted in a shutdown of nearly six months. Therefore, it is necessary to study the dynamic mechanical properties of this sandstone under freezing conditions and to develop a dynamic constitutive model to provide the basic mechanical parameters for engineering design.

Several studies have investigated the mechanical properties, damage evolution, and constitutive models in the statics of this rock. Yang et al. [7–9] systematically studied the static mechanical properties of water-rich soft rock. A common conclusion is that the strength and softening coefficient of such soft rock were low in unfrozen conditions, while the compressive strength and elastic modulus increased with a decrease in temperature in the frozen state. Wang [10–12] simulated the change process of the stress state of cretaceous frozen soft rock in underground construction via a testing method. In addition, a nonlinear creep constitutive model of frozen soft rock was proposed. Zhao et al. [13, 14] used the strain equivalent principle to study the damage evolution of such soft rocks under the triaxial compression test. Furthermore, a statistical damage constitutive model considering the residual deformation of sandstone was developed. However, in terms of dynamics, Liu and Xu [15, 16] conducted uniaxial impact tests on sandstone samples under different confining pressures. They found that the stress-strain curves under confining pressure

presented typical elastic-plastic characteristics. Zhu et al. [17, 18] investigated the failure process of sandstone from the perspective of microscopic crack propagation and energy absorption by using a split-Hopkinson pressure bar (SHPB) test device. In addition, the damage evolution was analyzed based on the statistical damage theory of the Weibull distribution. According to the characteristics of the stress-strain curves of soft rocks under impact loading, Zhao et al. [19, 20] modified the Zhu–Wang–Tang (Z–W–T) model by replacing the elastic element with a damaged body, after which a damage viscoelastic dynamic constitutive equation was derived. Yang et al. [21, 22] analyzed the variation in strength with temperature by combining SHPB systems with SEM. The microfracture mechanisms of saturated frozen red sandstone are explored. However, these studies mainly applied impact loading to sandstone samples at room temperature. Few studies have conducted experiments on rock behavior under low temperature, which is important for determining the significance and reference value for further research on the dynamic mechanical properties and constitutive model of cretaceous water-rich sandstone in the frozen state.

This paper aims to investigate the dynamic mechanical properties of saturated sandstone at different temperatures (20°C, −10°C, −20°C, and −30°C) using an SHPB pressure device. The dynamic constitutive model is established based on the stress-strain curves characteristics of the specimens. In addition, the applicability and rationality of the constitutive model are also verified using the experimental data. The results obtained can provide a reference and basis for the dynamic response, safety prediction, and support optimization of infrastructure under varying impact loads in cold regions.

2. Sandstone Impact Compression Test

2.1. Test Equipment. An SHPB device was used to study the dynamic mechanical properties of the specimens. The schematic and the main structures of the experiment device are shown in Figure 1.

The pressure bar of the system is alloy steel. The rod diameter is 50 mm, the elastic modulus is 210 GPa, and the longitudinal wave velocity is 5172 m/s. Pulse signals are collected using strain gauges on the incident and transmitted bars. The data acquisition system comprises a PC and an LK2107B ultrasonic dynamic strain gauge. The system can investigate the dynamic properties of rock, coal, concrete, and other materials under strain rates in the range 10^1~$10^3\ s^{-1}$.

2.2. Sample Preparation. The rocks were collected from the Quaternary cretaceous water-rich strata in the Wuju coal mine, Gansu province [23–25]. The rocks on-site were transported to the laboratory to process a standard rock sample with a diameter of 50 mm and a height-diameter ratio of 0.5, as shown in Figure 2. The basic physical and mechanical parameters are listed in Table 1. The specimens were selected first based on uniformity and integrity. Then, the UTA-2000A ultrasonic analyzer was used to select rock samples with similar longitudinal wave velocities as the test samples. All samples were placed inside a vacuum saturation machine to saturate the samples for 2 h, and the samples were then soaked in distilled water for more than 48 h to fully saturate the pores within the samples. After the saturation process, the specimens were placed into a low-temperature test freezer in subgroups for freezing at different temperatures.

2.3. Test Principle. The basic principle of the SHPB system is the propagation theory of stress waves in an elastic rod, which is based on the one-dimensional (1D) elastic wave hypothesis and uniformity hypothesis. Each cross section in the elastic rod is assumed to always remain planar when the stress wave propagates in the elastic rod in one dimension. According to the assumption of stress uniformity, the stress and strain are generally analyzed using the three-wave method:

$$\left.\begin{aligned} \sigma(t) &= \frac{E_c A_c}{2A_s}\left[\varepsilon_I(t) + \varepsilon_R(t) + \varepsilon_T(t)\right] \\ \varepsilon(t) &= \frac{C_c}{l_s}\int_0^t \left[\varepsilon_I(t) - \varepsilon_R(t) - \varepsilon_T(t)\right]\mathrm{d}t \\ \dot{\varepsilon}(t) &= \frac{C_c}{l_s}\left[\varepsilon_I(t) - \varepsilon_R(t) - \varepsilon_T(t)\right] \end{aligned}\right\}, \quad (1)$$

where $\varepsilon_I(t)$, $\varepsilon_R(t)$, and $\varepsilon_T(t)$ are the incident strain, the reflected strain, and the transmitted strain during impact, respectively; E_c, A_c, and C_c are the modulus of elasticity, the cross-sectional area, and the longitudinal wave velocity of the bar, respectively; and A_s and l_s are the cross-sectional area and the length of the sample, respectively.

2.4. Test Program. The range of blasting and impact loading strain rates for rock materials was 10~$10^3\ s^{-1}$ [26]. The temperature of low-temperature brine in the freezing system can reach −30°C in the western shaft freezing construction. Four temperatures were set for the test considering the temperature field distribution of the frozen wall, i.e., 20°C, −10°C, −20°C, and −30°C. The test results obtained at 20°C were considered to be the results of the comparative analysis group. The impact velocities of the striker were determined to be 3.0 m/s, 3.5 m/s, 3.8 m/s, 4.6 m/s, 5.2 m/s, and 6.0 m/s based on the monitoring data at different positions of the frozen wall during tunneling at the construction site. The impact tests on samples were repeated six times to ensure the accuracy of the test results considering the influence of the discreteness of the test data. For clear identification, the specimens were marked from *A* to *D*. For example, samples from −10°C were numbered B1-1~B1-6, ..., B6-1~B6-6. When the test was completed, the test data near the mean value were analyzed.

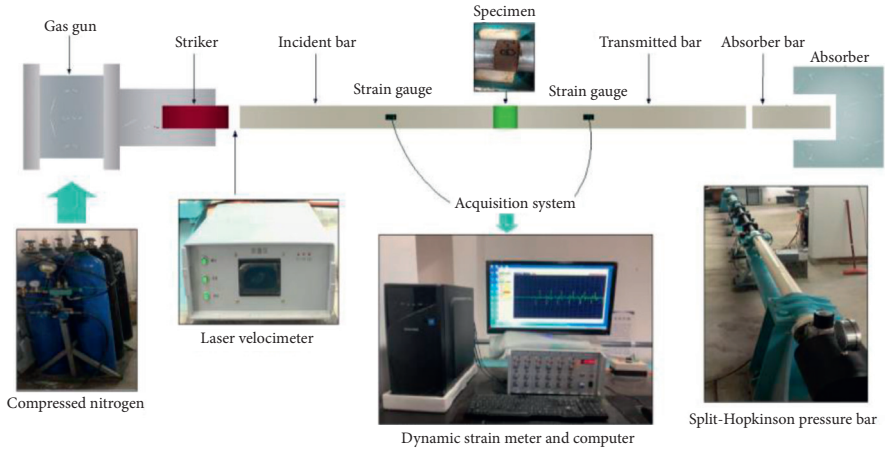

Figure 1: SHPB test system.

Figure 2: Standard sandstone samples.

3. Dynamic Analysis of Sandstone

3.1. Dynamic Stress-Strain Curve. A series of impact tests was conducted for different strain rates at different temperatures, i.e., 20°C, −10°C, −20°C, and −30°C. The stress-strain curves of the specimen can be obtained from these tests, as shown in Figure 3.

Figure 3 shows that the stress-strain curves of sandstone under impact loading can be divided into three distinct stages: (i) the first stage is the linear elastic deformation stage, where the relationship between the stress and strain is approximately linear. The slope represents the elastic deformation modulus of the rock. Figure 3 shows that the elastic deformation of sandstone is extremely small. (ii) The second stage is the plastic development stage. During this stage, the internal cracks of the sandstone begin to sprout and expand under impact loading. The slope of the curves in this stage is notably smaller than that of the first stage. Then, it decreases to 0 gradually. The results show that the stress reaches the maximum value at this stage. (iii) The third stage is the strain softening stage, in which the crack in the rock expands nonlinearly, and the stress decreases rapidly. Then, the specimen loses the capability of resistance to deformation.

A comparison of the stress-strain curves of sandstone at different tested temperatures demonstrates that the decreasing temperatures significantly influence the mechanical properties of the sandstone. (i) The strain at the translate point between the first and the second stages continues to decrease, while the strength continues to increase, indicating that the elasticity and brittleness of the rock are enhanced. In addition, the ability to resist the deformation of the rock is improved. (ii) In the second stage, the slope of the curves continues to decrease with temperature, indicating that the plasticity of the rock weakens and the brittleness increases. (iii) In the third stage, gradually, the rate of decline accelerated and the curves steepen. This indicates that the deformation ability of the rock is weakened from the peak strength point to the ultimate failure point at low temperatures. Evidently, the rock changes from extended brittleness to brittleness.

3.2. Relationship between Peak Stress and Strain Rate. Figure 4 shows the relationship between the peak stress and strain rate of sandstone under different temperatures.

Figure 4 shows that there is an increase in the peak stress with an increase in the strain rate. In addition, it indicates that the relationship between the peak stress and strain rate is a linear relationship, revealing that the relationship is an evident rate correlation. The peak stress of the specimen is the most sensitive to the strain rate at −10°C and the least sensitive to the strain rate at 20°C. It can be determined that the translate point occurs at 20°C, and this is believed to be because the water-rich cretaceous sandstone is soft and loose and has high porosity. The incident wave carries too much energy under high speed impact, resulting in the failure of the rock before the wave is fully passed into the transmission bar. Therefore, the extreme value appears because the transmitted wave signal collected by the system is less than the normal value.

The peak strength of the rock increases first and then decreases with the decrease in temperature, reaching a maximum at −20°C. The strength at −30°C is significantly lower than that of the samples at −20°C when the impact pressure is large, that is, under the action of high strain rates. The rule is the same as Yang's [27], which is due to the "frostbite effect" of sandstone under high strain rates.

Table 1: Properties of sandstone at room temperature.

Sample	Density (kg/m^3)	Porosity (%)	Longitudinal wave velocity (m/s)	Uniaxial compressive strength (MPa)	Poisson's ratio
Saturated	2182~2251	22.6~25.8	2419 ~ 2501	7.85~10.12	0.241~0.286

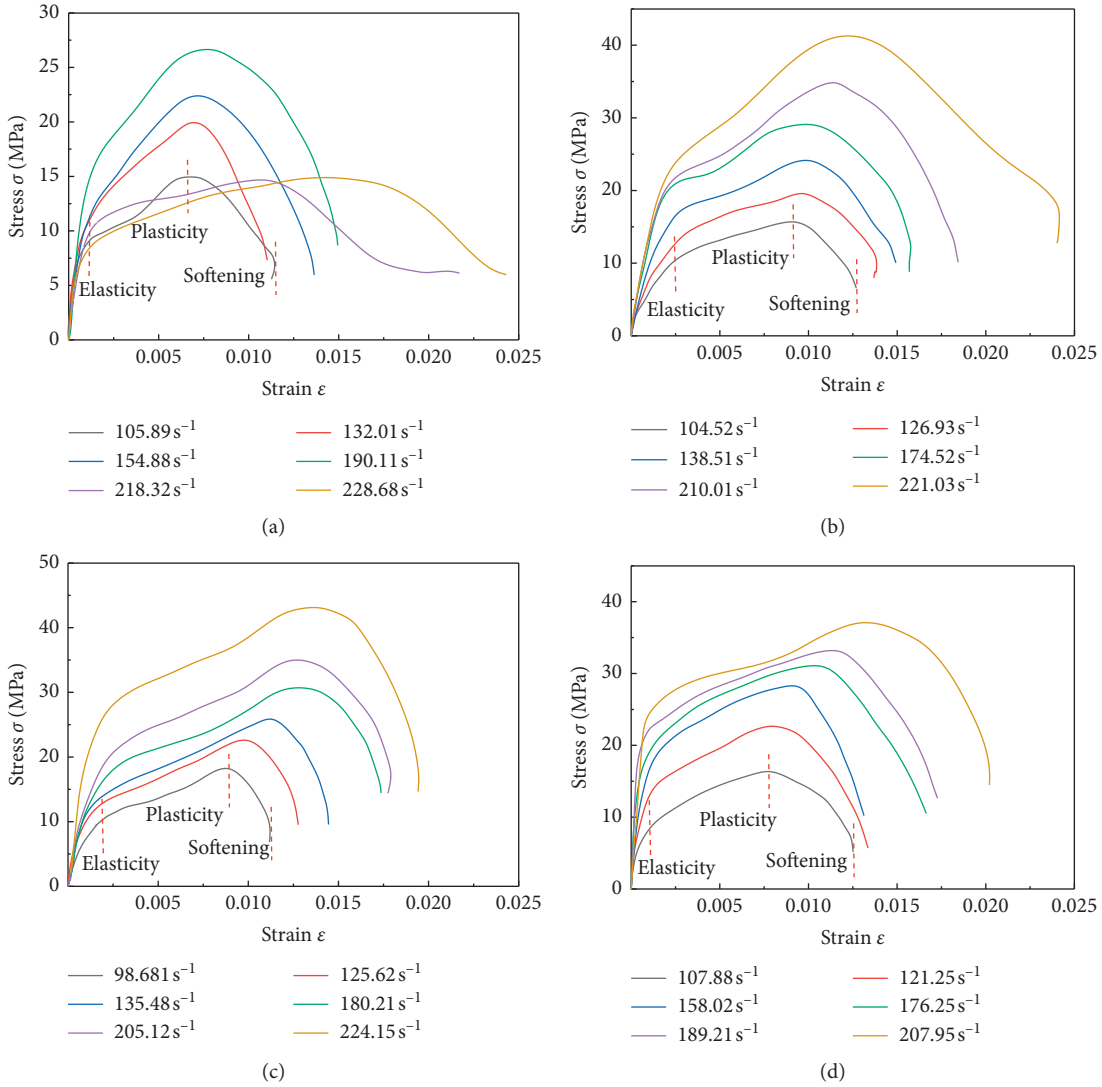

Figure 3: Stress-strain curves of sandstone at different temperatures: (a) $T = 20^{\circ}C$; (b) $T = -10^{\circ}C$; (c) $T = -20^{\circ}C$; (d) $T = -30^{\circ}C$.

3.3. Dynamic Elastic Modulus Analysis. The elastic modulus of the rock has an evident correction to the strain rate in the impact test. Therefore, the elastic modulus can be defined as the secant slope of 40%~60% or a tangent slope at 50% of the peak stress. Figure 3 shows that the stress-strain curve of frozen sandstone has an evident piecewise property and changes at different temperatures. Therefore, the methods above cannot be used for calculation. The tangent modulus of the elastic phase is used for analysis in this part, as shown in Figure 5.

Figure 5 shows that the dynamic elastic modulus increases with the decrease in temperature when $T \leq -10^{\circ}C$, where the growth rate from $-10^{\circ}C$ to $-20^{\circ}C$ is slow, while it is fast from $-20^{\circ}C$ to $-30^{\circ}C$. With the increase in impact loading, the difference of the elastic modulus between $-10^{\circ}C$ and $-20^{\circ}C$ decreases to 0 and then increases gradually, while there is a gradual increase in the difference of elastic modulus between $-20^{\circ}C$ and $-30^{\circ}C$. Comparing the range of variation of the elastic modulus of sandstone at different temperatures, it can be seen that the dynamic elastic modulus has the greatest sensitivity to the strain rate at $-30^{\circ}C$, while the sensitivity is basically the same at $-10^{\circ}C$ and $-20^{\circ}C$.

Based on the above analysis of the stress-strain curves, the brittleness of saturated sandstone increases, while the plasticity decreases with a decrease in temperature. According to the previous research results on the dynamic constitutive model of sandstone under room temperature, the dynamic constitutive model is established considering the temperature effect, strain rate effect, and damage effect

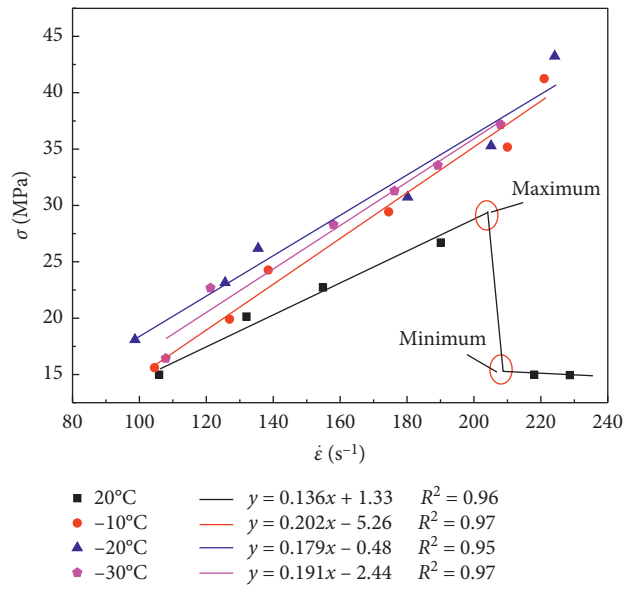

Figure 4: Relationship between peak stress and strain rate of sandstone under different temperatures.

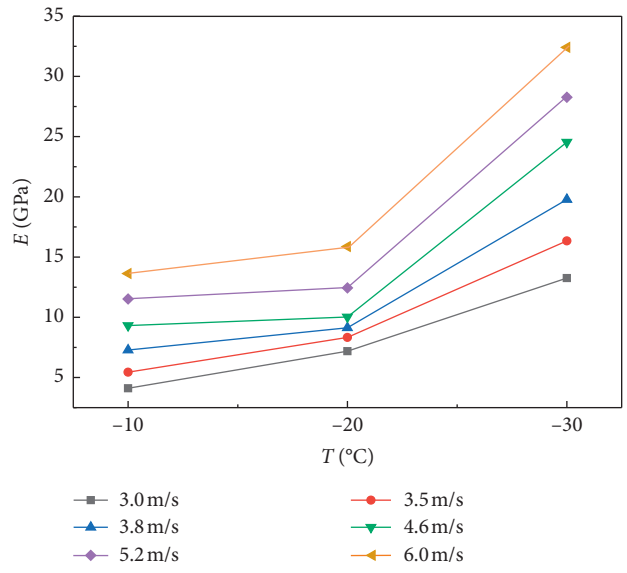

Figure 5: Dynamic elastic modulus of sandstone at different temperatures.

based on the Z–W–T model and theory of damage mechanics.

4. Establishment of Constitutive Model considering Temperature Effects

Tang et al. proposed the Z–W–T model [28], which is a dynamic constitutive model capable of describing the nonlinear viscoelastic responses of materials. This model was established based on homogeneous and isotropic simple material under 1D conditions. Based on the impact of polymer viscoelastic material, the Z–W–T model is composed of two different Maxwell bodies and a nonlinear spring. The constitutive model equation is as follows:

$$\sigma(t) = E_0\varepsilon(t) + \chi\varepsilon^2(t) + \kappa\varepsilon^3(t) + E_1\int_0^t \dot{\varepsilon}(t)\exp\left(-\frac{t-\tau}{\phi_1}\right)\mathrm{d}t + E_2\int_0^t \dot{\varepsilon}(t)\exp\left(-\frac{t-\tau}{\phi_2}\right)\mathrm{d}t, \quad (2)$$

where E_0 is the elastic modulus of the nonlinear spring; χ and κ are the nonlinear coefficients; E_1 and η_1 are the elastic modulus and viscosity coefficient of low-frequency linear spring, respectively; and E_2 and η_2 are the elastic modulus and viscosity coefficient of high-frequency linear spring, respectively.

The two different Maxwell bodies in the model describe the viscoelastic response under different strain rates, which act only on their own "effective responsible area" [29]. The response range of η_1 is 10^1~10^2 s^{-1}, and the response range of η_2 is 10^{-4}~10^{-6} s^{-1}. The relaxation time of the low-frequency Maxwell element is 10^1~10^2 s^{-1}. The loading time in the impact test is measured with a resolution of the order of several μs, there is therefore insufficient time to relax, and it is simplified as a simple spring.

According to the quasistatic compression test of saturated frozen sandstone, it can be obtained as follows: (i) the curves increase nonlinearly when $-10^{\circ}C \le T \le 20^{\circ}C$, so the polynomial part of the equilibrium stress independent of the strain rate in the Z–W–T equation can remain and represents the nonlinear elasticity; (ii) the curve increases linearly when $-30^{\circ}C \le T < -10^{\circ}C$, so only one term is considered in the polynomial part of the equilibrium stress independent of the strain rate in the Z–W–T equation, which is simplified in linear elasticity. Therefore, a viscoelastic constitutive model considering temperature effects is established. According to the response range of each Maxwell body in the Z–W–T model, the low-frequency part is replaced by a spring. The damaged body with elastic modulus E_D is increased. The simplified damage model is shown in Figure 6.

The spring E_0 is nonlinear when $-10^{\circ}C \le T \le 20^{\circ}C$. The constitutive model of the nonlinear elastomer I is

$$\sigma(t) = E_0\varepsilon(t) + \chi\varepsilon^2(t) + \kappa\varepsilon^3(t), \quad (3)$$

where $E_0 = E' + E''$ in which E' is the elastic modulus of low-frequency linear spring, E'' is the elastic modulus of the nonlinear elastic spring, and χ and κ are the nonlinear coefficients.

The spring E_0 is linear when $-30°C \le T < -10°C$. The nonlinear relation for elastomer I is

$$\sigma(t) = E_0\varepsilon(t). \quad (4)$$

To facilitate the analysis, the following assumptions are made regarding the model: (i) the rock interior is continuous, and the damage to the rock is homogeneous; (ii) the rock impact process is considered to be completed under constant strain rate loading conditions; and (iii) the strength of each microelement is subject to the Weibull distribution, and its probability density is as follows:

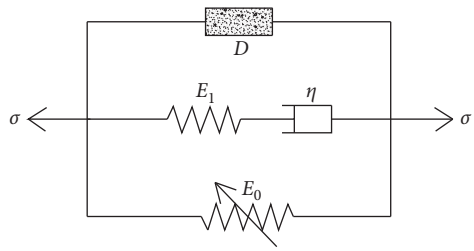

Figure 6: New nonlinear viscoelastic constitutive model.

$$\phi(\varepsilon) = \frac{m}{\alpha}\varepsilon^{m-1}\exp\left(-\frac{\varepsilon^m}{\alpha}\right), \tag{5}$$

where m and α are distributed parameters, and the size is related to the nature and shape of the material.

The degree of damage to the test piece is the sum of the defects contained in each microelement. The relationship between the damage variable D and the probability density of microelement failure can be given as follows:

$$\frac{\mathrm{d}D}{\mathrm{d}\varepsilon} = \phi(\varepsilon). \tag{6}$$

After integration,

$$D = 1 - \exp\left(-\frac{\varepsilon^m}{\alpha}\right). \tag{7}$$

From equation (7), the constitutive model of the damaged body II is

$$\sigma(t) = (1-D)E_D\varepsilon(t) = E_D\varepsilon(t)\exp\left(-\frac{\varepsilon^m}{\alpha}\right). \tag{8}$$

The Maxwell body comprises an elastic element and a damping element connected in series. The stress-strain relationship can be obtained as follows:

$$\sigma_1(t) = \sigma_{11}(t) = \sigma_{12}(t), \tag{9}$$

$$\varepsilon_1(t) = \varepsilon_{11}(t) + \varepsilon_{12}(t), \tag{10}$$

$$\sigma_{11} = E_1\varepsilon_{11}(t), \tag{11}$$

$$\sigma_{12} = \eta\dot{\varepsilon}_{12}(t). \tag{12}$$

Then, the derivative of equation (10) is found. Combining equations (9) and (11) with (12) yields

$$\dot{\varepsilon}(t) = \frac{\sigma_1'(t)}{E_1} + \frac{\sigma_1(t)}{\eta}. \tag{13}$$

The Laplace transform of equation (13) gives

$$L\left(\dot{\varepsilon}_1(t)\right) = L\left(\frac{\sigma_1'(t)}{E_1}\right) + L\left(\frac{\sigma_1(t)}{\eta}\right), \tag{14}$$

$$\frac{\dot{\varepsilon}_1}{S} = \frac{S\sigma_1(S) - \sigma_1(0)}{E_1} + \frac{\sigma_1(S)}{\eta}, \tag{15}$$

where $\sigma(0) = 0$. By substituting equation (15), the following can be obtained:

$$\sigma_1(S) = \eta\dot{\varepsilon}_1\left(\frac{1}{S} - \frac{1}{S + (E_1/\eta)}\right). \tag{16}$$

Laplace inverse transformations of equation (16) yield

$$L^{-1}\left(\sigma_1(S)\right) = \eta\dot{\varepsilon}_1 L^{-1}\left(\frac{1}{S} - \frac{1}{S + (E_1/\eta)}\right), \tag{17}$$

$$\sigma_1(t) = \eta\dot{\varepsilon}_1\left(1 - \exp\left(-\frac{E_1}{\eta}t\right)\right). \tag{18}$$

Substituting $t = (\varepsilon_1/\dot{\varepsilon}_1)$ into equation (18) gives

$$\sigma_1(t) = \eta\dot{\varepsilon}_1\left(1 - \exp\left(-\frac{E_1}{\eta}\frac{\varepsilon_1}{\dot{\varepsilon}_1}\right)\right). \tag{19}$$

Combined with equations (3), (4), and (19), the dynamic constitutive equation of saturated sandstone considering the damage effect, strain rate effect, and temperature effect is as follows:

$$\sigma = \begin{cases} E_0\varepsilon + \chi\varepsilon^2 + \kappa\varepsilon^3 + \eta\dot{\varepsilon}\left(1 - \exp\left(-\dfrac{E_1\varepsilon}{\eta\dot{\varepsilon}}\right)\right) + E_D\varepsilon\exp\left(-\dfrac{\varepsilon^m}{\alpha}\right), & T \in [20^\circ C, -10^\circ C], \\ E_0\varepsilon + \eta\dot{\varepsilon}\left(1 - \exp\left(-\dfrac{E_1\varepsilon}{\eta\dot{\varepsilon}}\right)\right) + E_D\varepsilon\exp\left(-\dfrac{\varepsilon^m}{\alpha}\right), & T \in (-10^\circ C, -30^\circ C]. \end{cases} \tag{20}$$

5. Test Verification of Constitutive Equation

There are eight unknown parameters in equation (20). The elastic modulus of each temperature sandstone can be first obtained from the static uniaxial test [30]. Then, the least-squares approximation theory is applied to fit the quasi-dynamic stress-strain curves at different temperatures in order to obtain E_0, E_1, χ, and κ from the constitutive equation. Finally, the stress-strain curves of impact tests under a high strain rate are fitted to determine the values of E_D, η, α, and m. Here, two sets of data at each temperature are selected for analysis.

The fitting curves for the prepeak stress and whole stress are given when $-10^\circ\mathrm{C} \le \mathrm{T} \le 20^\circ\mathrm{C}$, and the prepeak stress fitting curves are given when $-30^\circ\mathrm{C} \le \mathrm{T} < -10^\circ\mathrm{C}$. The fitting results are shown in Figure 7.

Figure 7 shows that the test curves are in good agreement with the fitting curves, where the correlation coefficient R^2 is 0.91487~0.99336. This indicates that the model is suitable for describing the dynamic mechanical constitutive model of

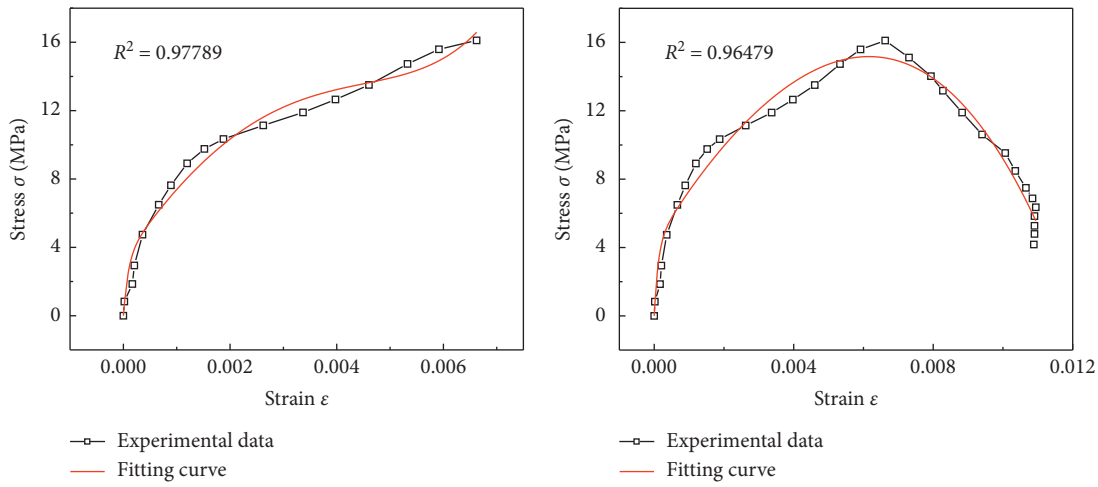

(a)

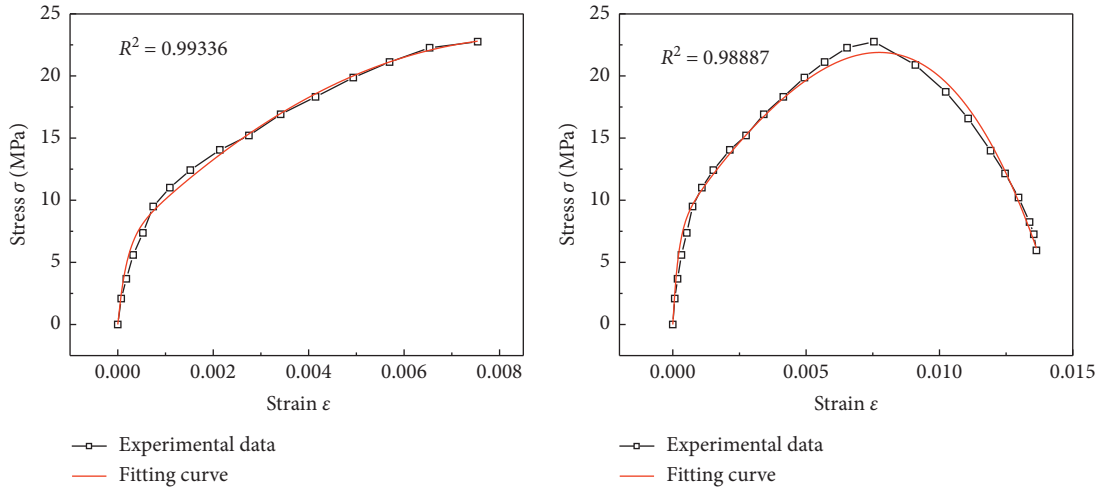

(b)

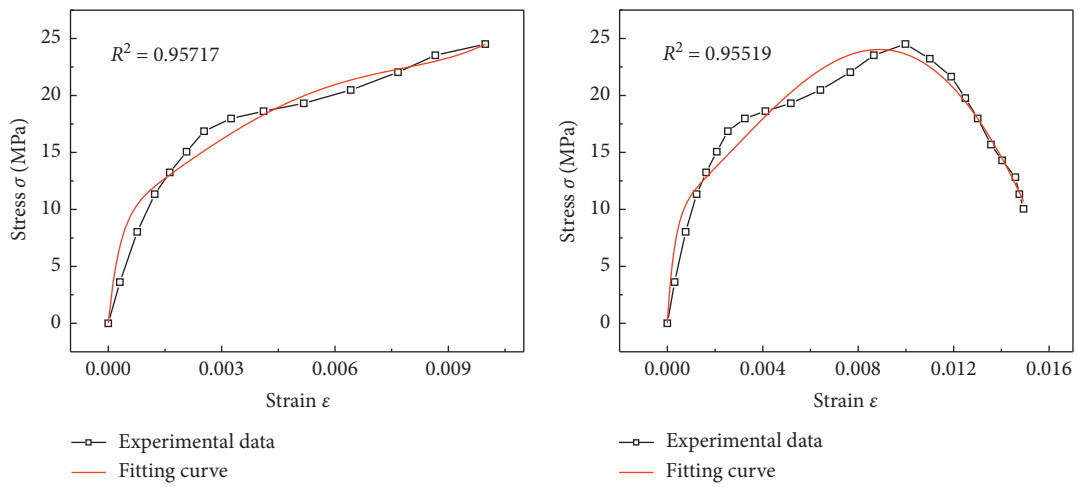

(c)

Figure 7: Continued.

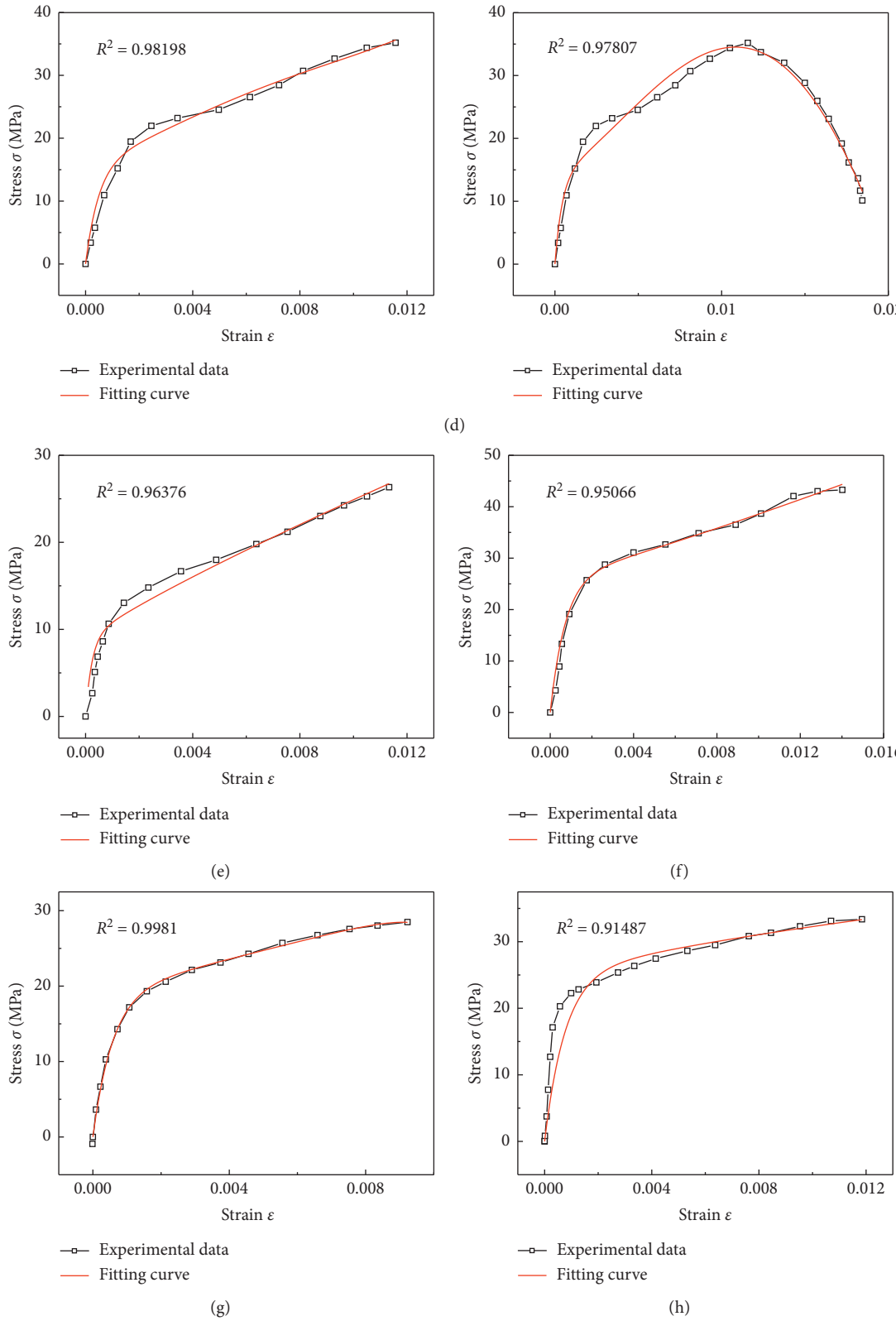

Figure 7: Dynamic stress-strain curve fitting of sandstone at different temperatures: (a) $T = 20^{\circ}C$ and $\dot{\varepsilon} = 105.89s^{-1}$; (b) $T = 20^{\circ}C$ and $\dot{\varepsilon} = 154.88s^{-1}$; (c) $T = -10^{\circ}C$ and $\dot{\varepsilon} = 138.5s^{-1}$; (d) $T = -10^{\circ}C$ and $\dot{\varepsilon} = 210s^{-1}$; (e) $T = -20^{\circ}C$ and $\dot{\varepsilon} = 135.48s^{-1}$; (f) $T = -20^{\circ}C$ and $\dot{\varepsilon} = 224.15s^{-1}$; (g) $T = -30^{\circ}C$ and $\dot{\varepsilon} = 158.02s^{-1}$; (h) $T = -30^{\circ}C$ and $\dot{\varepsilon} = 189.21s^{-1}$.

Table 2: Fitting parameters for sandstone with different strain rates at different temperatures.

T (°C)	$\dot{\varepsilon}$ (S^{-1})	E_0 (MPa)	χ	κ	E_1 (MPa)	E_D (MPa)	η_1 (S)	m	α (10^{-3})
20	105.89	3538.3	−841754.18	−6.61*E*7	36687.22	1065.138	0.031	0.967	0.004
						0.006	0.039	0.102	0.043
	154.88					18.781	0.042	0.228	0.053
						2.85*E*−4	0.048	0.083	0.039
−10	138.5	1557.32	−37815.56	−8.40*E*7	32020.66	212.34	0.069	0.535	0.023
						0.447	0.071	0.177	0.045
	210					0.208	0.076	0.177	0.041
						0.263	0.067	0.162	0.045
−20	135.48	585.696	—	—	36559.13	0.004	0.063	−0.017	0.088
	224.15					5.467*E*−4	0.117	0.019	0.057
−30	158.02	1138.09	—	—	32496.81	−2.81*E*−10	0.121	0.377	0.006
	189.21					−3.95*E*−5	0.131	0.024	0.055

saturated sandstone under different freezing temperatures. The fitting results of the whole stress-strain curves have an evident segmental phenomenon when $T \geq -10$°C. Therefore, it is possible to deduce the dynamic mechanical properties of sandstone during the whole impact process. The findings can give a better understanding of the shortcomings of the modified model, which can only partially address the pre-peak stress. Generally, the fitting accuracy of the stress part before the peak is slightly greater than the entire stress-strain curves. The stress yielding platform that appears during the impact process leads to a decrease in the fitting accuracy.

The parameters obtained by fitting the above constitutive equation are listed in Table 2.

From analyzing the values of each fitting parameter in Table 2, the value of E_0 is found to be 10^3, indicating that the elastic modulus obtained under static uniaxial loading is reasonable. E_1 is 10^4, which represents the elastic coefficient of the high-frequency Maxwell body, and is one order of magnitude larger than the numerical value of E_0, indicating that the response of sandstone under dynamic impact tests is more sensitive. The parameter m is always less than 1, and α is always less than 0.1. The relaxation time η_1 of sandstone is not constant, and it is correlated with temperature and strain rate. However, the range of the variation is small.

6. Conclusions

This study investigated the dynamic mechanical properties and constitutive model of frozen sandstone using a series of impact tests. The main conclusions drawn are summarized as follows:

(1) The dynamic stress-strain curves of low-temperature sandstone can be divided into three distinct stages: linear elastic deformation stage, plastic development stage, and strain softening stage. The peak stress is positively correlated with the strain rate, and the peak stress of the sample is most sensitive to the strain rate at −10°C. However, it is least sensitive to the strain rate at 20°C. The "frostbite effect" of the sandstone under high strain rates occurred at −30°C.

(2) The brittleness increases, and the plasticity decreases in the saturated sandstone with a decrease in the temperature. Based on the Z–W–T model, the following two points are considered: the characteristics of the stress-strain curves and the effects of the temperature and strain rate on the test results. A viscoelastic dynamic constitutive model of a nonlinear (or linear) body and Maxwell body in parallel with a damaged body is established. Furthermore, the microelement strength of the damaged body is defined based on the Weibull distribution.

(3) The new constitutive equations are used to fit the curves of sandstone with different strain rates at different temperatures. The fitted curves are in good agreement with the actual curves. The fitting result of the entire stress-strain curves can be employed to determine the dynamic mechanical properties of sandstone during the whole impact process when $T \geq -10$°C. This mitigates the shortcomings of the modified model, which only addresses the prepeak stress. By analyzing the rationality of each fitting parameter value in the constitutive equation, the applicability of the dynamic viscoelastic constitutive model to saturated sandstone is proven considering the effects of temperature, strain rate, and damage. The results reflect well the dynamic mechanical response of water-rich sandstone at different freezing temperatures, and they serve as reference for the related mechanical calculations.

Data Availability

The data sets generated and analyzed during the current study are available from the corresponding author on reasonable request.

Conflicts of Interest

The authors declare that there are no conflicts of interest regarding the publication of this paper.

Acknowledgments

This work was supported by the National Natural Science Foundation of China (nos. 51404193 and 41702339), the

Shanxi Provincial Natural Science Foundation (nos. 2018JQ4026 and S2015YFJQ1194), and the China Postdoctoral Fund (no. 2015M572581). The authors thank the Xi'an University of Science & Technology for providing the experiment conditions.

References

[1] W. M. Wang, L. Wang, and C. Q. Dai, "Frozen wall deformation analysis in weakly cemented soft rock based on layered calculation of strength," *Chinese Journal of Rock Mechanics and Engineering*, vol. S2, pp. 4110–4115, 2011.

[2] P. Yuan, N.-N. Wei, Q.-Y. Ma, and J.-C. Chang, "Coupled effect of water temperature and cyclic wetting and drying on dynamic mechanical characteristics of sandstone," *Advances in Civil Engineering*, vol. 2019, Article ID 8167651, 15 pages, 2019.

[3] H. Deng, Y. Zhang, Y. Zhi et al., "Sandstone dynamical characteristics influenced by water-rock interaction of bank slope," *Advances in Civil Engineering*, vol. 2019, Article ID 3279586, 11 pages, 2019.

[4] F. L. Zhang, Z. W. Zhu, T. T. Fu, and J. X. Jia, "Damage mechanism and dynamic constitutive model of frozen soil under uniaxial impact loading," *Mechanics of Materials*, vol. 140, Article ID 103217, 2020.

[5] M. Meng, Z. Sun, C. Wang, X. He, and Y. Xiao, "Size effect on mudstone strength during freezing-thawing cycle," *Environmental Geotechnics*, vol. 78, no. 15, pp. 435.1–435.14, 2019.

[6] D. Ma, Q. Ma, and P. Yuan, "SHPB tests and dynamic constitutive model of artificial frozen sandy clay under confining pressure and temperature state," *Cold Regions Science and Technology*, vol. 136, pp. 37–43, 2017.

[7] G. S. Yang, Y. Wei, and Y. J. Shen, "Mechanical behavior and strength forecast model of frozen saturated sandstone under triaxial compression," *Chinese Journal of Rock Mechanics and Engineering*, vol. 38, no. 4, pp. 683–694, 2019.

[8] H. M. Zhang, L. N. Lei, and G. S. Yang, "Characteristic and representative model of rock damage process under constant confining stress," *Journal of China University of Mining & Technology*, vol. 44, no. 1, pp. 59–63, 2015.

[9] H. Liu, G. S. Yang, and H. L. Jia, "Experimental study on meso-structure of rock in the process of crack (pore) water freezing," *Chinese Journal of Rock Mechanics and Engineering*, vol. 35, no. 12, pp. 2516–2524, 2016.

[10] R. H. Wang and W. Wang, "Analysis for features of the freezing temperature field under deflective pipes," *Chinese Journal of Geotechnical Engineering*, vol. 25, no. 6, pp. 658–661, 2003.

[11] D. W. Li, R. H. Wang, and J. H. Fan, "The nonlinear creep characteristics and parameter inversion of soft rock," *Journal of China Coal Society*, vol. 36, no. 3, pp. 388–392, 2011.

[12] J. Zhu, Y. Xu, and D. W. Li, "Experimental study of mechanical properties of frozen soft rock of Cretaceous formation in Bojianghaizi mine," *Journal of Jilin University (Earth Science Edition)*, vol. 46, no. 3, pp. 798–804, 2016.

[13] Z. H. Zhao, W. M. Wang, X. Gao, and J. X. Yan, "Triaxial compression damage characteristics of weakly cemented muddy soft rocks," *Journal of Zhejiang University (Engineering Edition)*, vol. 48, no. 8, pp. 1399–1405, 2014.

[14] Z.-H. Zhao, W.-M. Wang, C.-Q. Dai, and J.-X. Yan, "Failure characteristics of three-body model composed of rock and coal with different strength and stiffness," *Transactions of Nonferrous Metals Society of China*, vol. 24, no. 5, pp. 1538–1546, 2014.

[15] S. H. Liu and J. Y. Xu, "Mechanical and ultrasonic analysis on damage of sandstone under cyclic impact loading with confining pressure," *Journal of Vibration and Shock*, vol. 34, no. 1, pp. 190–194, 2015.

[16] H. Y. Wang, J. Y. Xu, P. Wang, S. Liu, and S. H. Liu, "Mechanical properties and energy mechanism of red sandstone under hydro-dynamic coupling," *Journal of Geotechnical Mechanics*, vol. 37, no. 10, pp. 2861–2868, 2016.

[17] J. J. Zhu, X. B. Li, F. Q. Gong, S. M. Wang, and W. He, "Experimental test and damage characteristics of sandstone under uniaxial impact compressive loads," *Journal of Central South University (Science and Technology)*, vol. 43, no. 7, pp. 2701–2707, 2012.

[18] B. Wang, X. B. Li, and T. B. Yin, "Split Hopkinson pressure bar (SHPB) experiments on dynamic strength of water-saturated sandstone," *Chinese Journal of Rock Mechanics and Engineering*, vol. 29, no. 5, pp. 1–3, 2010.

[19] G. M. Zhao, L. X. Xie, and X. R. Meng, "A constitutive model for soft rock under impact load," *Explosion and Shock Waves*, vol. 2, pp. 126–132, 2013.

[20] L. X. Xie, G. M. Zhao, and X. R. Meng, "Research on excess stress constitutive model of rock under impact load," *Chinese Journal of Rock Mechanics and Engineering*, vol. 32, no. S1, pp. 2772–2781, 2013.

[21] Y. Yang, R. S. Yang, J. G. Wang, S. Z. Fang, and N. N. Zhang, "Experimental study on dynamic mechanical properties of red sandstone under low temperatures," *Journal of China Coal Society*, vol. 43, no. 4, pp. 967–975, 2018.

[22] Y. Yang, J. G. Wang, and R. S. Yang, "Analysis of deformation and fracture of the saturated frozen red sandstone under high strain rate," *Journal of Rock Mechanics and Engineering*, vol. 37, no. S2, pp. 4016–4026, 2018.

[23] H. M. Zhang, X. Z. Meng, and G. S. Yang, "A study on mechanical properties and damage model of rock subjected to freeze-thaw cycles and confining pressure," *Cold Regions Science and Technology*, vol. 174, Article ID 103056, 2020.

[24] Y. J. Shen, H. W. Yang, J. M. Xi, Y. Yang, Y. Z. Wang, and X. Wei, "A novel shearing fracture morphology method to assess the influence of freeze-thaw actions on concrete-granite interface," *Cold Regions Science and Technology*, vol. 169, Article ID 102900, 2019.

[25] H. L. Jia, S. Ding, Y. Wang, F. Zi, Q. Sun, and G. S. Yang, "An NMR-based investigation of pore water freezing process in sandstone," *Cold Regions Science and Technology*, vol. 168, Article ID 102893, 2019.

[26] H. Y. Liu, S. R. Lv, L. M. Zhang, and X. P. Yuan, "A dynamic damage constitutive model for a rock mass with persistent joints," *International Journal of Rock Mechanics and Mining Sciences*, vol. 75, pp. 132–139, 2015.

[27] Y. Yang and R. S. Yang, "'Frostbite effect' of red sandstone under high strain rates," *Chinese Journal of Engineering Sciences*, vol. 41, no. 10, pp. 1249–1257, 2019.

[28] Z. Zhu, G. Kang, Y. Ma, Q. Xie, D. Zhang, and J. Ning, "Temperature damage and constitutive model of frozen soil under dynamic loading," *Mechanics of Materials*, vol. 102, pp. 108–116, 2016.

[29] N. Liang, J. Dai, and X. Liu, "Study on tensile damage constitutive model for multiscale polypropylene fiber concrete," *Advances in Materials Science and Engineering*, vol. 2016, Article ID 9168984, 6 pages, 2016.

[30] R. L. Shan, Y. W. Song, L. W. Song, and Y. Bai, "Dynamic property tests of frozen red sandstone using a split Hopkinson pressure bar," *Earthquake Engineering and Engineering Vibration*, vol. 18, no. 3, pp. 511–519, 2019.